

Article

# Micron-Sized Hierarchical Beta Zeolites Templated by Mesoscale Cationic Polymers as Robust Catalysts for Acylation of Anisole with Acetic Anhydride

Songsong Miao<sup>1,2</sup>, Shuaishuai Sun<sup>1</sup>, Zhenyu Lei<sup>1</sup>, Yuting Sun<sup>1</sup>, Chen Zhao<sup>1</sup>, Junling Zhan<sup>1</sup>, Wenxiang Zhang<sup>1</sup> and Mingjun Jia<sup>1,\*</sup> 

<sup>1</sup> Key Laboratory of Surface and Interface Chemistry of Jilin Province, College of Chemistry, Jilin University, Changchun 130012, China; kidcrest@ciac.ac.cn (S.M.); sunshuaishuai1997@163.com (S.S.); leizy22@mails.jlu.edu.cn (Z.L.); syt15354685582@163.com (Y.S.); zc07072023@163.com (C.Z.); zhanjl\_96@163.com (J.Z.); zhwenx@jlu.edu.cn (W.Z.)

<sup>2</sup> Changchun Institute of Applied Chemistry, Chinese Academy of Sciences, Changchun 130022, China

\* Correspondence: jiamj@jlu.edu.cn; Tel.: +86-431-85168420

**Abstract:** Hierarchical Beta zeolites with interconnected intracrystalline mesopores and high structural stability are highly attractive for catalytic applications involving bulky reactants. Here, by introducing a suitable amount of polydiallyldimethylammonium chloride into the initial synthesis system, micron-sized Beta zeolite crystals with abundant hierarchical porosity (Beta-H) were hydrothermally synthesized. The sample named Beta-H\_1 exhibited very high catalytic activity and durability for the Friedel–Crafts acylation of anisole with acetic anhydride. A 92% conversion rate of acetic anhydride could be achieved after 1 h of reaction in a fixed bed reactor, and 71% conversion still remained after 10 h, much better than the rate for conventional Beta zeolite (which decreased rapidly from 85% to 37% within 10 h). The enhanced catalytic performance of Beta-H zeolites could be mainly attributed to the relatively lower strong acid density and the faster transport rate of the hierarchical zeolites. In addition, Beta-H showed high structural stability and could be easily regenerated via high-temperature calcination without obvious loss in catalytic activity, demonstrating its great potential for catalytic applications in the industrially important Friedel–Crafts acylation process.

**Keywords:** zeolite; acylation; hierarchical; high stability; intracrystalline mesopore



**Citation:** Miao, S.; Sun, S.; Lei, Z.; Sun, Y.; Zhao, C.; Zhan, J.; Zhang, W.; Jia, M. Micron-Sized Hierarchical Beta Zeolites Templated by Mesoscale Cationic Polymers as Robust Catalysts for Acylation of Anisole with Acetic Anhydride. *Catalysts* **2023**, *13*, 1517. <https://doi.org/10.3390/catal13121517>

Academic Editor: Antonio Eduardo Palomares

Received: 15 November 2023

Revised: 13 December 2023

Accepted: 17 December 2023

Published: 18 December 2023



**Copyright:** © 2023 by the authors. Licensee MDPI, Basel, Switzerland. This article is an open access article distributed under the terms and conditions of the Creative Commons Attribution (CC BY) license (<https://creativecommons.org/licenses/by/4.0/>).

## 1. Introduction

Friedel–Crafts acylation of aromatics is an industrially important reaction in manufacturing aromatic ketones, which are key intermediates for producing fine chemicals, agrochemicals, pharmaceuticals, and fragrances [1,2]. Traditionally, acylation processes are mainly carried out in the presence of stoichiometric amounts of anhydrous metal halides such as AlCl<sub>3</sub> and FeCl<sub>3</sub> [3]. However, there are some serious limitations in these conventional homogeneous Lewis acid catalysis processes with respect to environmental concerns and resource utilization, mainly arising from the disposal of the huge amount of metal halides and toxic wastes. In order to meet the demands of green chemical industry, recent efforts have been devoted to exploring heterogeneous acylation catalysts, including supported heteropolyacid [4–6], solid superacid [7], carbon-based metal oxides [8,9], and zeolites [10–20].

Among the various investigated zeolite catalysts, zeolite Beta with \*BEA topology has received more attention, due mainly to its relatively high catalytic activity and excellent structural stability [3]. Two commercial processes based on the application of zeolite Beta in the industrial production of 4-methoxyacetophenone and 3,4-dimethoxyacetophenone have already been realized through the acylation of anisole and veratrole with acetic anhydride [21]. In spite of this progress, however, the zeolite Beta-catalyzed acylation

reactions still need improvements, e.g., to deal with the rapid deactivation of the zeolites caused by the deposition of heavy reaction products within the pores or on the external surface of the zeolite crystallites.

Previous literature works have demonstrated that the fabrication of hierarchical pores (mesopores and/or macropores) in microporous zeolites might be an effective way to decrease the deactivation rate in various acid-catalyzed reactions, including catalytic cracking, alkylation, and acylation reactions [22–25]. As reported in the literature, hierarchical Beta zeolites could be synthesized by introducing some organic compounds as mesoporous templates [26–28]. However, the resultant mesopores present in these hierarchical Beta zeolites are usually made of secondary particle-piled pores or built with amorphous pore walls [29–33]. In this case, an obvious decrease in the structural stability of the hierarchical zeolite framework is commonly detected during the catalytic reaction process (including regeneration via high-temperature calcination), thus leading to a gradual decrease in catalytic acylation activity with increasing the number of recycling times [12,34,35].

Alternatively, hierarchically porous Beta zeolites containing intracrystalline mesopores may be synthesized by using some mesoporous carbon materials as hard templates [25,36,37]. The structural stability of these kinds of hierarchical Beta zeolites is higher, owing to the formation of crystalline framework walls of the mesoporous system. However, some drawbacks are still present concerning the complexity of synthesis procedures and the high cost of the hard template. Recently, some low-cost polycations such as polydiallyldimethylammonium chloride (PDAD) have been widely used as surface stabilizers or growth modifiers to tailor the structure and morphology of metal nanoparticles and porous materials [38–41]. For instance, Xiao and co-authors reported that hierarchical Beta zeolite containing intracrystalline mesopores could be synthesized by using PDAD as a mesoscale template [40,41]. The interconnected mesopores with zeolitic crystal walls bring about excellent hydrothermal stability for the generated hierarchical Beta zeolites, thus leading to the formation of highly active and stable catalysts for several acid-catalyzed reactions involving the activation of large molecules, such as the alkylation of benzene with benzyl alcohol and the condensation of benzaldehyde with glycerol. This progress clearly reveals the great potential of polycations like PDAD in creating hierarchical zeolite Beta with desirable features for application in various industrially important catalytic processes.

Recently, we and our co-workers carried out some works on modulating the morphology, porosity, and particle size of zeolite crystals [42–45]. By optimizing the usage amount of PDAD, hierarchical TS-1 zeolites with abundant intracrystalline mesopores could be obtained, and the resultant zeolites exhibit much higher catalytic activity and recyclability than the conventional TS-1 zeolites for the catalytic oxidation of bulky organosulfur compounds [42]. It was also found that the deactivation rate of Beta zeolites could be decreased somewhat by reducing the crystalline size or introducing intercrystalline mesopores, which are derived from the usage of additional additives like Triton X-100 (polyethylene glycol tert-octylphenyl ether) or PDAD in the synthesis systems [35,45].

Here, we report the synthesis and catalytic application of a kind of micron-sized hierarchical Beta zeolite (Beta-H) with abundant mesopores and suitable strong acid density. By adjusting the sol–gel composition and the addition amount of PDAD, the condition-optimized zeolite named Beta-H\_1 showed enhanced catalytic activity and a decreased deactivation rate for the acylation of anisole with acetic anhydride. In particular, the catalytic activity of the spent zeolite Beta-H\_1 could be fully recovered by consecutive high-temperature calcination, confirming the excellent structural stability of the micron-sized hierarchical Beta zeolites.

## 2. Results and Discussion

### 2.1. Catalyst Characterization

Figure 1 shows the XRD patterns of various Beta zeolites prepared by adding different amounts of PDAD. The conventional Beta-C sample exhibits the characteristic diffraction peaks of the \*BEA structure at  $2\theta$  angles of  $7.8^\circ$  and  $22.5^\circ$ . The three Beta-H<sub>*n*</sub> samples

show the same diffraction patterns as the Beta-C sample, confirming the phase purity of the PDAD-mediated Beta-H<sub>*n*</sub> zeolites. Among them, Beta-H<sub>1</sub>, derived from the usage of a relatively low amount of PDAD, shows the strongest diffraction peaks, demonstrating the high crystallinity of the sample, which is defined as 100% relative crystallinity (RC). With a further increase in the addition amount of PDAD, the relative crystallinities of the resultant samples (Beta-H<sub>2</sub> and Beta-H<sub>3</sub>) decrease somewhat (about 70%, Table 1) but are still comparable with that of the conventional Beta-C zeolite.

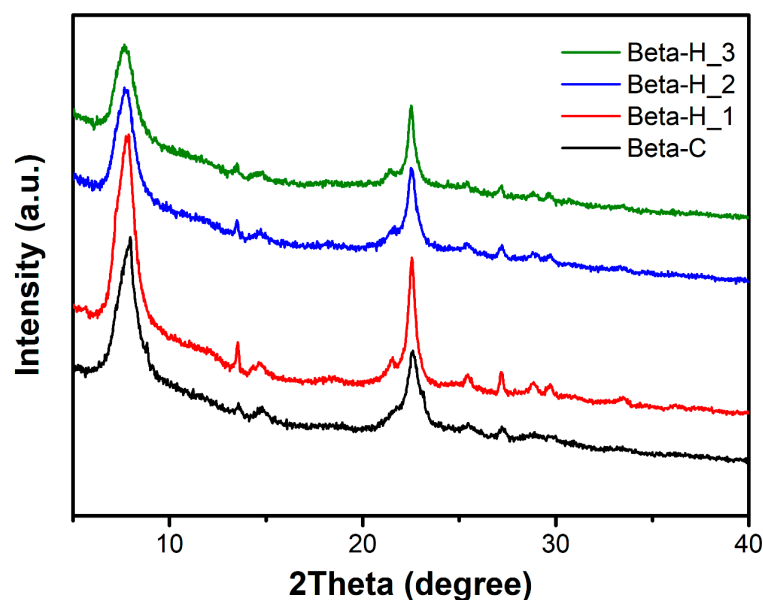


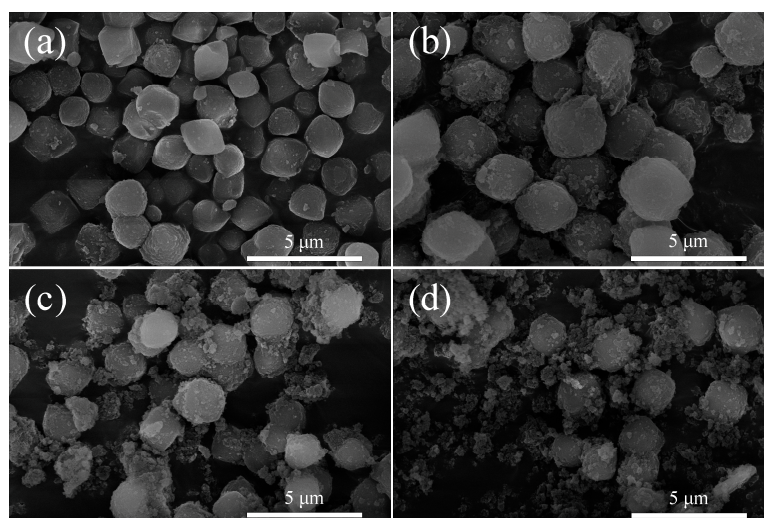
Figure 1. The XRD patterns of Beta-H<sub>*n*</sub> and Beta-C zeolites.

Table 1. Compositions and textural parameters of various Beta zeolites.

Samples	Si/Al <sup>a</sup>	S <sub>BET</sub> (m <sup>2</sup> /g)	S <sub>micro</sub> (m <sup>2</sup> /g)	V <sub>micro</sub> (cm <sup>3</sup> /g)	V <sub>meso</sub> (cm <sup>3</sup> /g)	Yield <sup>d</sup> (%)	RC <sup>e</sup> (%)
Beta-C	21.3	532	453	0.23	0.32	73	77
Beta-H <sub>1</sub>	18.5	574	447	0.23	0.78	74	100
Beta-H <sub>2</sub>	19.3	555	375	0.19	0.69	74	73
Beta-H <sub>3</sub>	20.4	517	311	0.16	1.18	76	69

<sup>a</sup> Measured via ICP; <sup>b</sup> Calculated using the *t*-plot method; <sup>c</sup> Calculated using the BJH method (from adsorption); <sup>d</sup> Based on the mass of fumed silica used; <sup>e</sup> Relative crystallinity (RC): calculated by comparing the sum of the intensity of peaks at 2θ = 7.8 and 22.5°.

SEM images of the Beta-C and Beta-H<sub>*n*</sub> zeolites are shown in Figure 2. It can be seen that zeolite Beta-C exhibits a smooth surface morphology with an average particle size of 1.3~1.7 μm (Figure 2a). Compared with that of Beta-C, the particle size of the Beta-H<sub>1</sub> zeolite is larger (mostly above 2.1 μm). With a further increase in the addition amount of PDAD, the resultant Beta-H<sub>2</sub> and Beta-H<sub>3</sub> become non-uniform; a considerable amount of smaller particles can be observed besides the micron-sized zeolite crystals. These results suggest that the addition of a small amount of PDAD does not have an obvious effect on the formation of micron-sized Beta zeolite (i.e., Beta-H<sub>1</sub>), while a higher amount of PDAD may have a negative effect on the formation of large zeolite crystals.



**Figure 2.** SEM images of (a) Beta-C, (b) Beta-H\_1, (c) Beta-H\_2, and (d) Beta-H\_3.

The nitrogen adsorption–desorption isotherms of various Beta zeolites are presented in Figure 3a, and the textural properties of these zeolites are summarized in Table 1. The isotherm of Beta-C is of type I, with a steep uptake at relative pressure below 0.01. The rapid rise at  $p/p_0 > 0.95$  should be related to the presence of a small amount of particle-piled macropores in Beta-C. For the three Beta-H<sub>*n*</sub> samples, an obvious hysteresis loop appears from 0.6 to 0.9 ( $p/p_0$ ), assignable to the capillary condensation of nitrogen in mesopores. At a higher relative pressure above 0.9, the curves continue to rise without reaching a plateau, corresponding to the filling of interparticle voids between the smaller zeolite particles. The inset in Figure 3a reveals the presence of a relatively high amount of mesopores ranging from 5 to 25 nm. According to the related literature, such mesopores might be mainly derived from the release of voids within the zeolite crystals filled by the cationic polymer after calcination [40]. The TEM images of Beta-C and Beta-H\_1 show the lattice fringes with consistent orientations, indicating the single crystalline nature of the zeolites (Figure 3b,c). For the other two samples (Beta-H\_2 and Beta-H\_3), a relatively rough surface with different lattice orientations was detected, further confirming the nonuniformity of these two zeolites as already revealed by the SEM measurements. From the detailed data listed in Table 1, a drop in the micropore volume from 0.23 cm<sup>3</sup>/g to 0.16 cm<sup>3</sup>/g can be seen with an increase in the PDAD addition amount, accompanied with an increase in mesopore volume. It should be mentioned here that it is unusual to synthesize micron-sized Beta zeolite crystals with hierarchical porosity, since most of the previously reported synthesis approaches commonly generate hierarchical Beta zeolites with smaller crystalline size (0.10–0.60 μm) and relatively poor stability [41,46]. Here, Beta-H\_1 has a much larger crystal size (2.1 μm) compared with the literature-reported hierarchical Beta zeolites, including the one with an average crystal size of 0.6 μm synthesized by Wang et al. using a similar approach (with TEOH and PDAD as co-templates) [40,47]. The main difference between our work and the literature work is that a relatively low addition amount of TEOH (with a TEOH/SiO<sub>2</sub> ratio of 0.20) was adopted in the present case, while a much higher TEOH/SiO<sub>2</sub> ratio of 0.68 was used in the literature work [47]. These results suggest that optimizing the sol–gel composition is quite an important factor for adjusting the porosity and crystal size of the hierarchical Beta zeolites.

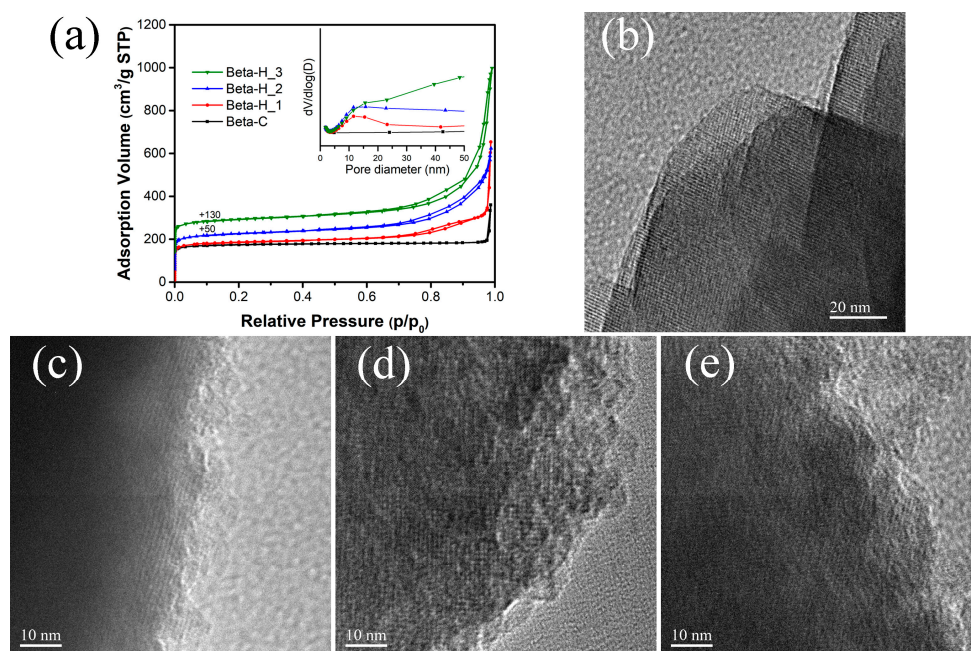


**Figure 3.** (a) The nitrogen adsorption–desorption isotherms of various Beta zeolites. The inset is the pore size distribution curves calculated from the adsorption branch (BJH). (b–e) High-resolution TEM images of the Beta-C, Beta-H\_1, Beta-H\_2, and Beta-H\_3 zeolites, respectively.

The acidic properties of various Beta zeolites were studied by means of  $\text{NH}_3$ -TPD measurement and FT-IR spectroscopy. The  $\text{NH}_3$ -TPD profiles of all samples show two major desorption peaks at about  $190^\circ\text{C}$  and  $350^\circ\text{C}$  (Figure 4), which represent the weak acid sites and strong acid sites, respectively. Among them, conventional Beta-C possesses the largest amount of strong acid sites, and the strong acid density decreases in the order of  $\text{Beta-C} > \text{Beta-H}_1 > \text{Beta-H}_2 > \text{Beta-H}_3$ . Moreover, it can also be observed that increasing the PDAD addition amount led to a gradual shift of the high-temperature desorption peak towards lower temperatures (from  $356^\circ\text{C}$  to  $340^\circ\text{C}$ ). These results suggest that both the density and strength of the strong acid centers in the resultant Beta-H zeolites could be tuned to a certain extent through changing the usage amount of PDAD in the initial synthesis sol–gel system.

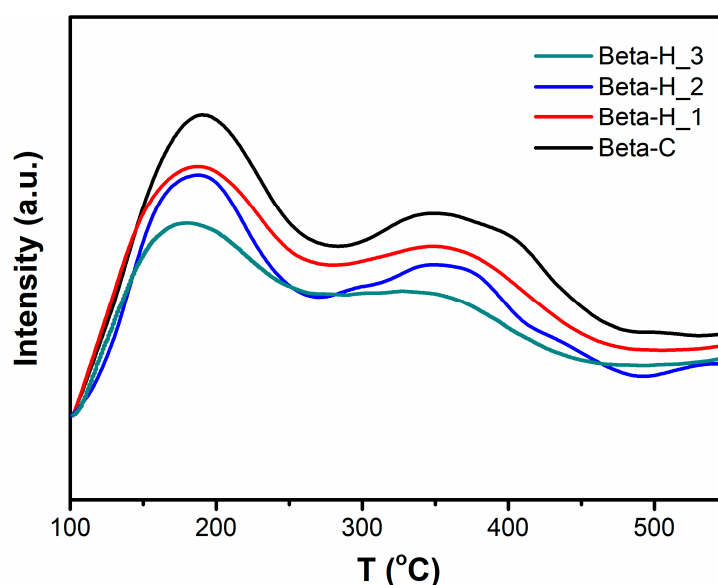


**Figure 4.**  $\text{NH}_3$ -TPD profiles of conventional Beta zeolite and hierarchical Beta zeolites.

Figure 5 depicts the FT-IR spectra of the hydroxyl groups in various Beta zeolites. Three major vibration bands appear in the region, namely, partially framework-connected Al-OH (band at  $3778\text{ cm}^{-1}$ ), Si-OH (band at  $3733\text{ cm}^{-1}$ ), and the Brønsted acidic bridging Si-OH-Al (band at  $3602\text{ cm}^{-1}$ ) [48–50]. An increase in absorbance at  $3778\text{ cm}^{-1}$  and  $3733\text{ cm}^{-1}$  can be observed with increasing PDAD content, suggesting that the addition of PDAD may lead to the formation of more defects in the zeolite crystals, in line with the appearance of mesopores within the zeolite crystals [48,50]. The peak intensity of the Brønsted acidic sites decreases with increasing PDAD content, following the same order as described in the  $\text{NH}_3$ -TPD results.

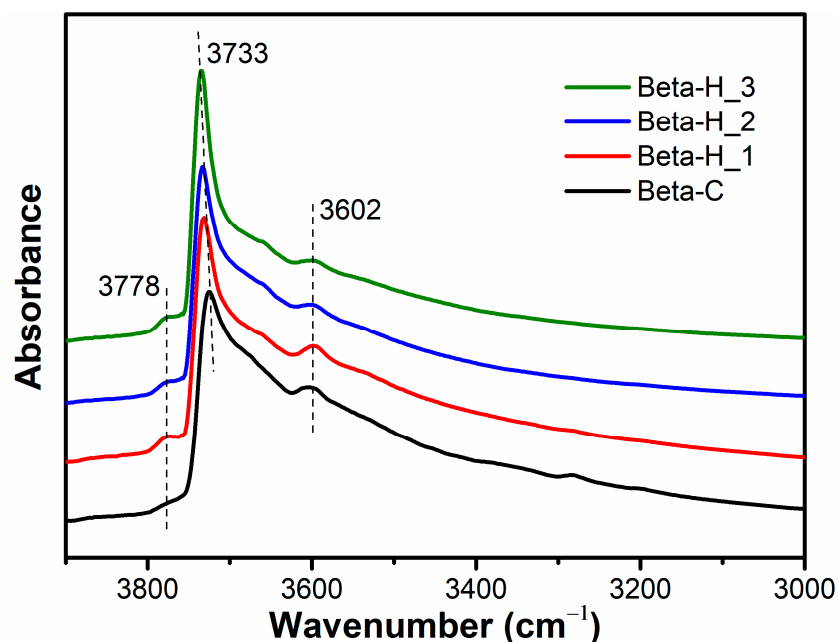


Figure 5. FT-IR spectra of hydroxyl groups in various Beta zeolites.

The above characterization results demonstrate that hierarchical Beta zeolites with different porosities, crystal sizes, and acidities could be obtained by changing the addition amount of the co-template PDAD in the initial synthesis system. As the texture parameters, including the acidity, of the zeolites are the key factors influencing their catalytic properties for various acid catalysis processes, it seems reasonable to expect that the catalytic performance of these Beta-H<sub>n</sub> zeolites could be tuned to a certain extent in the acylation of anisole with acetic anhydride.

## 2.2. Catalysis Test

### 2.2.1. Acylation of AN with AA in a Batch Reactor

The catalytic properties of various Beta zeolites were first investigated for the acylation of AN with AA carried out in a round-bottom flask. In the present case, all the acylation reactions were achieved with quite high selectivity (>99%, without consideration of the deposited carbonaceous species on the catalysts) to the main product of 4-methoxyacetophenone (4-MAP), in line with the results reported in the literature [12,17,35]. Table S1 shows the main catalytic results for the various Beta zeolites in the acylation reactions with different AA/AN ratios (i.e., 1/6 and 1/1).

In the anisole-rich system (AA/AN = 6/1), all the Beta-H<sub>n</sub> zeolites present relatively higher catalytic activities than that of Beta-C, while Beta-H<sub>1</sub> gave the highest AA conversion (66%) after 1 h of reaction. The difference in the catalytic activities of the above zeolite catalysts is not significant under such test conditions, due mainly to the fact that the excessive AN could also act as a solvent to inhibit the rapid deactivation of the zeolites by avoiding the fast accumulation of heavier products. Their catalytic activities decreased

drastically when a lesser amount of AN was used. When a stoichiometric ratio of reactants was adopted ( $AA/AN = 1/1$ ), an obvious difference in the catalytic performance between the hierarchical Beta-H<sub>n</sub> zeolites and Beta-C was detected. The AA conversion over Beta-H<sub>n</sub> zeolites is much higher than that over the conventional one, showing that Beta-H<sub>1</sub> is the most efficient catalyst in the equimolar reaction system. Apparently, the growth trend of the AA conversion over Beta-C declines more quickly in comparison with that over the hierarchical Beta-H zeolites, implying that the deactivation rate of Beta zeolites could be decreased to some extent by generating more mesopores within the zeolite crystals.

### 2.2.2. Acylation of AN with AA in a Fixed Bed Reactor

The catalytic behaviors of Beta-C and Beta-H<sub>1</sub> in a fixed bed reactor were also comparatively studied. It should be mentioned that during the first 15 min, the concentration of 4-MAP in the collected products was quite low over both zeolites, which could be explained by the strong adsorption of the ketone products on the zeolites.

As shown in Figure 6a, both the Beta-H<sub>1</sub> and Beta-C zeolites exhibit very high initial activity with an AA conversion rate of about 90%. A rapid drop in activity can be observed over Beta-C with time on stream, as the AA conversion decreased from 85% to 37% after 10 h of reaction. During the same reaction period, the hierarchical Beta-H<sub>1</sub> sample showed a much lesser deactivation rate than Beta-C, along with a gradual decrease in AA conversion from 92% to 71%. According to the related literature [51], it is believed that the strong Brønsted acidic sites in zeolites are the main active sites for the acylation of AN with AA, while the weak acidic sites (normally present on the external surface of the zeolites) make little contribution. In this case, the rapid deactivation of the Beta-C zeolite could be mainly assigned to the inefficient mass transportation of the micropore system, as well as the easier poisoning of the stronger acidic sites by the formed ketone products. On the other hand, the relatively low deactivation rate of Beta-H<sub>1</sub> can be mainly attributed to the presence of abundant interconnected mesopores that can improve the accessibility of active sites and facilitate the mass transfer and diffusion of bulky molecules within the zeolite channels. Moreover, the relatively low density of the strong acid sites in Beta-H<sub>1</sub> should also be helpful for suppressing the formation of heavier products, including some carbonaceous deposits [5,52].

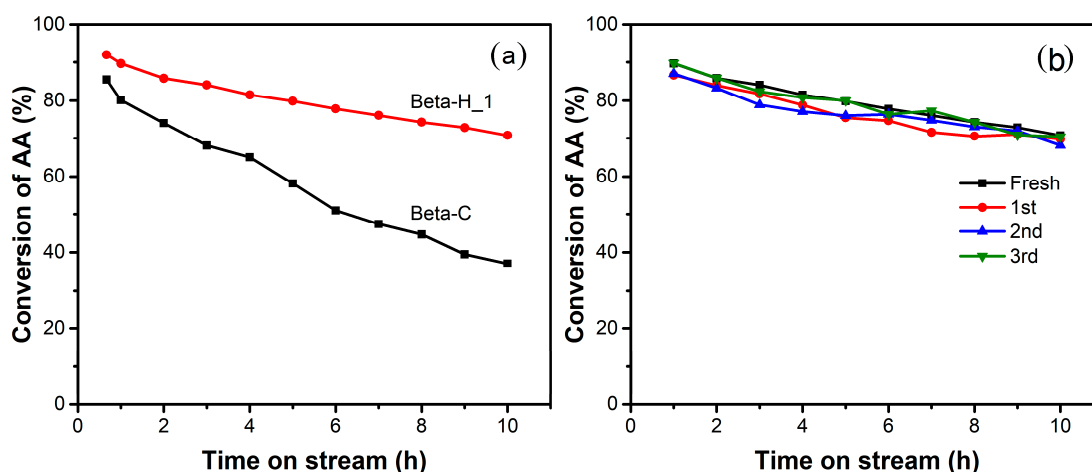


**Figure 6.** (a) Conversion of AA over Beta-C and Beta-H<sub>1</sub> as a function of time on stream in the acylation of anisole with acetic anhydride; (b) recycling study on Beta-H<sub>1</sub> after regeneration by calcination in air. Reaction conditions:  $AA/AN = 1/5$  (mol/mol), reactant mixture flow rate of 0.08 mL/min, nitrogen flow rate of 23 mL/min, temperature of 90 °C.

The reusability of Beta-H<sub>1</sub> zeolite was also examined. As shown in Figure 6b, the catalytic activity of the spent Beta-H<sub>1</sub> was fully recovered by calcination in air flow at 580 °C for 4 h, and no obvious loss in activity was detected after three successive

regeneration cycles. This feature is quite valuable for the Beta zeolites with hierarchical porosity, since previously reported hierarchical Beta zeolites derived via other synthesis strategies commonly suffered from a gradual loss in catalytic activity with an increasing number of regeneration cycles [12,34,35,41,53].

To further elucidate the deactivation phenomenon in this process, an equimolar reaction mixture of AA and AN (1:1) was also adopted to accelerate the deactivation of the zeolite catalysts in a fixed bed reactor. As illustrated in Figure S1, both the Beta-C and Beta-H\_1 zeolites showed steeply decreasing activity in 6 h of time on stream, with loss of the initial catalytic activities (based on the AA conversion after a 40 min reaction) of around 80% and 63%, respectively.

Various characterizations were then conducted to gain insight into the evolution of the catalysts underlying the deactivation phenomenon. Figure 7 depicts the TGA curves of the spent catalysts. The weight loss in the range of 40 to 150 °C could be mainly assigned to the desorption of the physically adsorbed water and ethanol (as the washing solvent) on the zeolites. The weight loss between 150 and 700 °C can be attributed to the removal of the adsorbed reagents (i.e., acetic anhydride and anisole), the aromatic ketone products, and the coke-like deposits trapped in the channels or on the surface of the zeolite catalysts [52,54]. By comparing the weight loss rates in the higher-temperature region, which were 9.0% and 7.7% for Beta-C and Beta-H\_1, respectively, it was found that less carbonaceous deposits were present on the Beta-H\_1 zeolite over the same reaction period. Moreover, the N<sub>2</sub> adsorption–desorption results, shown in Figure S2, reveal that an obvious decrease in N<sub>2</sub> uptake (below  $p/p_0 < 0.01$ ) occurred in both spent zeolite catalysts, while the loss of the microporous volume in the spent Beta-C was more serious compared with that in the spent Beta-H\_1 catalyst (with remaining micropore volumes of 43% vs. 56%, Table 2). In addition, the hysteresis loop of the spent Beta-H\_1 is smaller than that of the fresh Beta-H\_1, suggesting that a portion of the mesopores in the zeolites were also filled by some carbonaceous deposits. Considering the fact that zeolite Beta-H\_1 has a larger crystal size than the conventional Beta-C zeolite, it could be deduced that the presence of rich intracrystalline mesopores in Beta-H\_1 plays a determinative role in improving the diffusion capability for both reagents and products, thus effectively decreasing the deposition rate in the zeolite by the fast transportation of coke-like precursors out of the larger zeolite crystal.

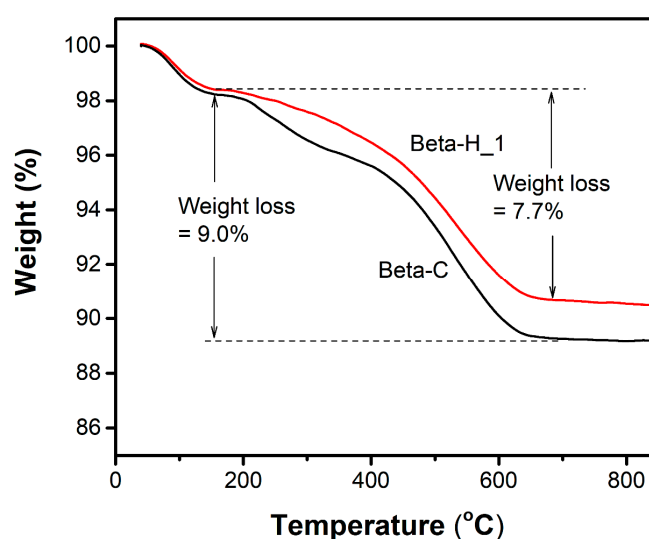


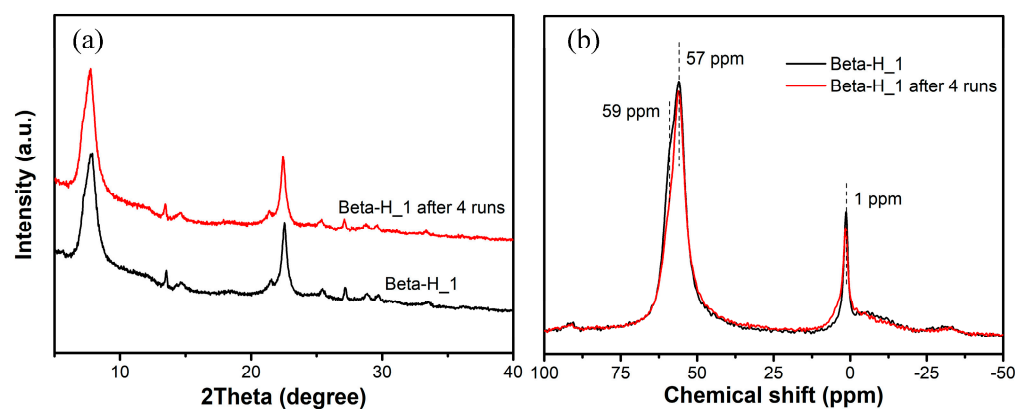
Figure 7. TGA curves of Beta-C and Beta-H\_1 after reaction in the fixed bed reactor.

**Table 2.** Textural parameters of the Beta-C and Beta-H\_1 zeolites before and after use.

Samples	$S_{\text{BET}}$ (m <sup>2</sup> /g)	$S_{\text{micro}}$ <sup>a</sup> (m <sup>2</sup> /g)	$V_{\text{micro}}$ <sup>a</sup> (cm <sup>3</sup> /g)	$V_{\text{meso}}$ <sup>b</sup> (cm <sup>3</sup> /g)
Beta-C	532	453	0.23	0.32
spent Beta-C	237	186 (41%) <sup>c</sup>	0.10 (43%) <sup>c</sup>	0.11
Beta-H_1	574	447	0.23	0.78
spent Beta-H_1	354	250 (56%) <sup>c</sup>	0.13 (56%) <sup>c</sup>	0.77

<sup>a</sup> Calculated using the *t*-plot method. <sup>b</sup> Calculated using the BJH method (from adsorption). <sup>c</sup> The numbers in the parentheses represent the percentages of  $S_{\text{micro}}$  or  $V_{\text{micro}}$  content left in the catalysts.

Some additional characterization results such as XRD and <sup>27</sup>Al MAS NMR results further demonstrated the high structural stability of the Beta-H\_1 catalyst. The XRD pattern (Figure 8a) and a SEM image (Figure S3) of the regenerated Beta-H\_1 show negligible change in comparison with the pristine sample. The <sup>27</sup>Al MAS NMR spectra shown in Figure 8b reveal that the coordination environments of Al species in the regenerated Beta-H\_1 zeolite are well consistent with those in the fresh catalyst, since both the major signal (57 ppm) related to the tetrahedrally coordinated framework Al and the weak signal assigned to the octahedrally coordinated extra-framework Al (0 ppm) remain well after the catalytic tests and regenerated treatment [55,56]. The FT-IR result reveals a slight decrease in the peak intensity of the Brönsted acidic sites (bridging OH groups at 3602 cm<sup>-1</sup>) after consecutive catalyst regeneration (Figure S4a), which is in line with the NH<sub>3</sub>-TPD result (Figure S4b). The slight loss in the stronger acidic sites of the zeolite catalysts can be explained by the inevitable detachment of a small part of bridging OH groups (related to the framework Al species) after undergoing repeated regeneration treatments at higher calcination temperatures (580 °C, air flow) [57,58].

**Figure 8.** (a) XRD patterns and (b) <sup>27</sup>Al MAS NMR spectra of Fresh Beta-H\_1 and regenerated Beta-H\_1 after 4 catalytic runs.

### 3. Materials and Methods

#### 3.1. Chemicals and Materials

Fumed silica (Aerosil 200, 99.8%, Degusa, Germany), sodium aluminate (NaAlO<sub>2</sub>, chemically pure, Sinopharm, China), sodium hydroxide (NaOH, 96%, Sinopharm, China), tetraethylammonium hydroxide (TEAOH, 25 wt% aqueous solution, Alfa Aesar, China), and polydiallyldimethylammonium chloride (PDAD, 35 wt% aqueous solution, Aldrich, USA) were used in the preparation of Beta zeolite. Ammonium nitrate (NH<sub>4</sub>NO<sub>3</sub>, 99%, Beijing Chemical Reagent, China) was used for ion exchange in the zeolites. Acetic anhydride (AA, 98.5%, Sinopharm, China) and anisole (AN, 99%, Sinopharm, China) were used for catalytic tests. All the above materials were used as purchased, without purification.

### 3.2. Catalyst Preparation

Hierarchical Beta zeolites (Beta-H) were hydrothermally synthesized in the presence of the TEOAH template and the PDAD polymer according to the procedure reported in the literature [47], but with a much lower content of TEOAH in the initial sol–gel system. The molar composition of the synthesis gel was 1.0 SiO<sub>2</sub>: 0.025 Al<sub>2</sub>O<sub>3</sub>: 0.06 Na<sub>2</sub>O: 0.20 TEOAH: 15 H<sub>2</sub>O. Typically, 0.224 g of NaOH, 0.328 g of NaAlO<sub>2</sub>, 14.5 g of water, and 9.4 g of TEOAH aqueous solution (25 wt.%) were mixed and stirred, followed by the addition of 4.8 g of fumed silica. A viscous gel was formed after stirring for 5 h; a certain amount of PDAD solution (1.0, 2.0, or 3.0 g for Beta-H\_1, Beta-H\_2, and Beta-H\_3, respectively) was then added into the gel, which was stirred at 80 °C for 3 h. After that, the mixture was transferred into a stainless autoclave equipped with a Teflon liner and hydrothermally crystallized at 150 °C for 5 days (to obtain Beta-H\_1 and Beta-H\_2) or 7 days (to obtain Beta-H\_3). The solid products were separated by filtration, washed with deionized water, dried at 80 °C, and then calcined at 550 °C for 6 h in air to remove the template.

Conventional Beta zeolite (Beta-C) was synthesized by using the same procedure and the same sol–gel composition as described above, just without the addition of PDAD.

The protonic-form zeolite Beta was obtained by ion exchange with 1.0 M NH<sub>4</sub>NO<sub>3</sub> solution at 80 °C for 5 h. After the ion exchange process, the samples were filtered, dried, and calcined at 550 °C. Unless otherwise stated, H-form Beta zeolites were used for the following characterizations and catalytic tests.

### 3.3. Characterizations

Powder X-ray diffraction (XRD) measurements were carried out using an Empyrean X-ray Diffractometer from PANalytical B.V., (Netherlands) with Cu K $\alpha$  radiation ( $\lambda = 1.5418 \text{ \AA}$ ) operated at 40 mA and 40 kV. The diffraction patterns were recorded in the  $2\theta$  range of 5–40°. The N<sub>2</sub> adsorption–desorption experiments were performed on a Micromeritics ASAP 2010N analyzer (USA) at –196 °C; prior to the measurements, the samples were degassed at 300 °C for 4 h. Scanning electron microscope (SEM) images were captured with a Hitachi X-65 electron microscope (Japan). Transmission electron microscope (TEM) images were collected on a Jeol Jem-2100F (Japan) at an accelerating voltage of 200 kV. The Si/Al ratios of the samples were determined by means of inductively coupled plasma–atomic emission spectroscopy (ICP-AES) using a PerkinElmer emission spectrometer (USA). Thermogravimetric analyses were carried out on a NETZSCH STA499F3 QMS403D\Bruker V70 analyzer (Germany) from ambient temperature to 850 °C at a heating rate of 10 °C/min<sup>–1</sup> under an air flow of 60 mL/min. The acidity of the catalysts was determined by temperature-programmed desorption of ammonia (NH<sub>3</sub>-TPD) measurement on a Xianquan TP5079 multi-purpose adsorption instrument (China). For each measurement, 50 mg of zeolite (40–60 mesh) was pretreated at 500 °C in helium gas for 1 h. After cooling down to 100 °C, the gas flow was switched to 10% NH<sub>3</sub>/He for the adsorption of ammonia for 30 min, then the sample was flushed with He gas to remove physisorbed NH<sub>3</sub>. The desorption was carried out in the temperature range of 100–550 °C with a heating rate of 10 °C/min, and the signal was recorded using a TCD detector. Fourier transform infrared spectroscopy (FT-IR) spectra were recorded on a Thermo Scientific Nicolet™ 6700 spectrometer (USA). The samples were first pressed into self-supporting wafers, then placed into the vacuum cell and heated at 350 °C for 2 h under vacuum. After cooling down to room temperature, the spectra were collected at 4 cm<sup>–1</sup> resolution. <sup>27</sup>Al MAS NMR of the fresh and regenerated Beta zeolites was performed on a Bruker AVANCE III 600 spectrometer (Germany) equipped with a 4 mm triple resonance probe operating at a resonance frequency of 156.4 MHz. The chemical shifts of <sup>27</sup>Al were referenced to 1 mol/L aqueous Al(NO<sub>3</sub>)<sub>3</sub>.

### 3.4. Catalytic Tests

The acylation of anisole with acetic anhydride was first carried out in a round-bottom flask equipped with a reflux condenser. Typically, 10 mmol AA and 60 mmol AN were mixed (AA/AN = 1/6), then 200 mg of catalyst was added to the mixture before the reaction

started in an 80 °C oil bath. In some cases, an equimolar reaction mixture containing 35.5 mmol AA and 35.5 mmol AN was also used for evaluating the catalytic performance of the zeolite catalysts. Small aliquots were withdrawn from the reaction mixture periodically and filtered with a filter membrane for analysis.

In addition, the catalytic behaviors of the representative Beta zeolites were also investigated in a fixed bed continuous down-flow reactor at atmospheric pressure. In general, 500 mg of catalyst (40–60 mesh) sandwiched between quartz wools was loaded in a quartz-tube reactor placed in a vertical furnace. Prior to the reaction, the catalyst was activated in air flow (30 mL/min) at 550 °C for 1 h; then the air flow was switched to N<sub>2</sub> gas flow (23 mL/min). After decreasing the temperature of the catalyst bed to 90 °C, the reactant mixture containing AA and AN (in a molar ratio of 1/1 or 1/5) was pumped into the reactor by a micropump at a flow rate of 0.08 mL/min to start the reaction. The products were collected at the bottom of the quartz tube hourly using a cold trap for analysis, and they were analyzed using a gas chromatograph (Shimadzu GC-8A, Japan) equipped with a flame ionization detector (FID) and an HP-5 capillary column (30 m × 0.25 mm, Agilent, USA). A recycling test on the zeolite was conducted after the used catalyst was regenerated by means of calcination in air flow at 580 °C for 4 h.

### 3.5. Analysis of the Spent Catalysts

After 6 h on stream (AA/AN = 1/1), ethanol was pumped into the reactor to extract the soluble organics out of the zeolite channels, and this procedure lasted for 5 h at an ethanol flow of 0.16 mL/min. The spent catalysts were then dried at 110 °C for 1 h before further characterization. Nitrogen adsorption–desorption measurement was carried out to determine the BET surface area and pore volume of the spent zeolites. Prior to measurement, the spent catalyst was outgassed at 120 °C for 4 h. The total amount of carbonaceous species deposited in the zeolite was determined using thermogravimetric analysis (TGA). About 10 mg of sample was heated from room temperature to 850 °C under flowing air with a heating rate of 10 °C/min.

## 4. Conclusions

In summary, micron-sized hierarchical Beta zeolites were synthesized by adding a suitable amount of PDAD into a conventional hydrothermal synthesis system. The resultant hierarchical Beta-H possessed abundant intracrystalline mesoporosity and lower strong acid density than the conventional Beta-C zeolite. The condition-optimized Beta-H zeolite with micron-size crystal particles presented enhanced catalytic activity and a lower deactivation rate for the acylation of anisole with acetic anhydride in comparison with the conventional Beta zeolite. The deactivated catalyst was fully recovered by consecutive calcination treatment without an obvious loss in catalytic activity, demonstrating the excellent structural stability of the micron-sized hierarchical Beta zeolite. We believe that this work will be helpful to the development of more efficient zeolite Beta catalysts with robust stability and regeneration performance for catalytic applications in Friedel–Crafts acylation reactions.

**Supplementary Materials:** The following supporting information can be downloaded at: <https://www.mdpi.com/article/10.3390/catal13121517/s1>, Figure S1: Conversion of AA over Beta-C and Beta-H\_1 as a function of time on stream in acylation of anisole with acetic anhydride. Reaction conditions: AA/AN = 1/1 (mol/mol), reactant mixture flow rate of 0.08 mL/min, nitrogen flow rate of 23 mL/min, temperature of 90 °C; Figure S2: Comparison of nitrogen adsorption–desorption isotherms of fresh and spent BetaH\_1 zeolites; Figure S3: SEM images of (a) fresh Beta-H\_1 and (b) regenerated Beta-H\_1 after 4 catalytic runs; Figure S4: (a) NH<sub>3</sub>-TPD profiles and (b) FT-IR spectra of fresh Beta-H\_1 and regenerated Beta-H\_1 after 4 catalytic runs; Table S1: Catalytic results of Friedel–Crafts acylation of AN with AA over different zeolites.

**Author Contributions:** Conceptualization, S.M.; methodology, S.M.; formal analysis, S.S., Z.L. and Y.S.; investigation, C.Z. and J.Z.; writing—original draft preparation, S.M.; writing—review and editing, M.J.; supervision, W.Z. and M.J.; funding acquisition, M.J. All authors have read and agreed to the published version of the manuscript.

**Funding:** This research was funded by the National Nature Science Foundation of China (22172058) and Sino-High (China) Co., Ltd. (201922000200038).

**Data Availability Statement:** Data are contained within the article or supplementary material.

**Conflicts of Interest:** The authors declare no conflict of interest.

## References

1. Jana, S.K. Advances in liquid-phase Friedel–Crafts acylation of aromatics catalyzed by heterogeneous solids. *Catal. Surv. Asia* **2006**, *10*, 98–109. [[CrossRef](#)]
2. Sartori, G.; Maggi, R. Use of Solid Catalysts in Friedel–Crafts Acylation Reactions. *Chem. Rev.* **2006**, *106*, 1077–1104. [[CrossRef](#)]
3. Bejblova, M.; Prochazkova, D.; Cejka, J. Acylation reactions over zeolites and mesoporous catalysts. *ChemSusChem* **2009**, *2*, 486–499. [[CrossRef](#)]
4. Cardoso, L.A.M.; Alves, W., Jr.; Gonzaga, A.R.E.; Aguiar, L.M.G.; Andrade, H.M.C. Friedel–Crafts acylation of anisole with acetic anhydride over silica-supported heteropolyphosphotungstic acid (HPW/SiO<sub>2</sub>). *J. Mol. Catal. A Chem.* **2004**, *209*, 189–197. [[CrossRef](#)]
5. Sarsani, V.; Lyon, C.; Hutchenson, K.; Harmer, M.; Subramaniam, B. Continuous acylation of anisole by acetic anhydride in mesoporous solid acid catalysts: Reaction media effects on catalyst deactivation. *J. Catal.* **2007**, *245*, 184–190. [[CrossRef](#)]
6. Parida, K.M.; Mallick, S.; Pradhan, G.C. Acylation of anisole over 12-heteropolyacid of tungsten and molybdenum promoted zirconia. *J. Mol. Catal. A Chem.* **2009**, *297*, 93–100. [[CrossRef](#)]
7. Arata, K.; Nakamura, H.; Shouji, M. Friedel–Crafts acylation of toluene catalyzed by solid superacids. *Appl. Catal. A Gen.* **2000**, *197*, 213–219. [[CrossRef](#)]
8. Zhang, H.; Song, X.; Hu, D.; Zhang, W.; Jia, M. Iron-based nanoparticles embedded in a graphitic layer of carbon architectures as stable heterogeneous Friedel–Crafts acylation catalysts. *Catal. Sci. Technol.* **2019**, *9*, 3812–3819. [[CrossRef](#)]
9. Zhang, H.; Song, X.; Zhao, C.; Hu, D.; Zhang, W.; Jia, M. N-Doped Porous Carbon–FeC Nanoparticle Composites as Catalysts for Friedel–Crafts Acylation. *ACS Appl. Nano Mater.* **2020**, *3*, 6664–6674. [[CrossRef](#)]
10. Padmanabhan, A.; Selvin, R.; Hsu, H.L.; Xiao, L.W. Efficient Acylation of Anisole over Hierarchical Porous ZSM-5 Structure. *Chem. Eng. Technol.* **2010**, *33*, 988–1002. [[CrossRef](#)]
11. Inagaki, S.; Imai, H.; Tsujiuchi, S.; Yakushiji, H.; Yokoi, T.; Tatsumi, T. Enhancement of catalytic properties of interlayer-expanded zeolite Al-MWW via the control of interlayer silylation conditions. *Microporous Mesoporous Mater.* **2011**, *142*, 354–362. [[CrossRef](#)]
12. Kore, R.; Srivastava, R.; Satpati, B. Synthesis of industrially important aromatic and heterocyclic ketones using hierarchical ZSM-5 and Beta zeolites. *Appl. Catal. A Gen.* **2015**, *493*, 129–141. [[CrossRef](#)]
13. Wei, H.; Xie, S.; Gao, N.; Liu, K.; Liu, X.; Xin, W.; Li, X.; Liu, S.; Xu, L. Alkali treatment upon MCM-49 zeolite with various contents of HMI in the presence of CTAB and application in anisole acylation with acetic anhydride. *Appl. Catal. A Gen.* **2015**, *495*, 152–161. [[CrossRef](#)]
14. Kim, J.-C.; Cho, K.; Lee, S.; Ryoo, R. Mesopore wall-catalyzed Friedel–Crafts acylation of bulky aromatic compounds in MFI zeolite nanosponge. *Catal. Today* **2015**, *243*, 103–108. [[CrossRef](#)]
15. Xu, L.; Ji, X.; Li, S.; Zhou, Z.; Du, X.; Sun, J.; Deng, F.; Che, S.; Wu, P. Self-Assembly of Cetyltrimethylammonium Bromide and Lamellar Zeolite Precursor for the Preparation of Hierarchical MWW Zeolite. *Chem. Mater.* **2016**, *28*, 4512–4521. [[CrossRef](#)]
16. Aleixo, R.; Elvas-Leitão, R.; Martins, F.; Carvalho, A.P.; Brigas, A.; Martins, A.; Nunes, N. Kinetic study of Friedel–Crafts acylation reactions over hierarchical MCM-22 zeolites. *Mol. Catal.* **2017**, *434*, 175–183. [[CrossRef](#)]
17. Huang, G.; Ji, P.; Xu, H.; Jiang, J.-G.; Chen, L.; Wu, P. Fast synthesis of hierarchical Beta zeolites with uniform nanocrystals from layered silicate precursor. *Microporous Mesoporous Mater.* **2017**, *248*, 30–39. [[CrossRef](#)]
18. Makihara, M.; Aoki, H.; Komura, K. Reaction Profiles of High Silica MOR Zeolite Catalyzed Friedel–Crafts Acylation of Anisole Using Acetic Anhydride in Acetic Acid. *Catal. Lett.* **2018**, *148*, 2974–2979. [[CrossRef](#)]
19. Silva, D.S.A.; Castelblanco, W.N.; Piva, D.H.; de Macedo, V.; Carvalho, K.T.G.; Urquieta-González, E.A. Tuning the Brønsted and Lewis acid nature in HZSM-5 zeolites by the generation of intracrystalline mesoporosity—Catalytic behavior for the acylation of anisole. *Mol. Catal.* **2020**, *492*, 111026. [[CrossRef](#)]
20. Hu, W.-H.; Liu, M.-N.; Luo, Q.-X.; Zhang, J.; Chen, H.; Xu, L.; Sun, M.; Ma, X.; Hao, Q.-Q. Friedel–Crafts acylation of anisole with acetic anhydride over single- to multiple-layer MWW zeolites: Catalytic behavior and kinetic mechanism. *Chem. Eng. J.* **2023**, *466*, 143098. [[CrossRef](#)]
21. Kantam, M.L.; Ranganath, K.V.S.; Sateesh, M.; Kumar, K.B.S.; Choudary, B.M. Friedel–Crafts acylation of aromatics and heteroaromatics by beta zeolite. *J. Mol. Catal. A Chem.* **2005**, *225*, 15–20. [[CrossRef](#)]
22. Kerstens, D.; Smeyers, B.; Van Waeyenberg, J.; Zhang, Q.; Yu, J.; Sels, B.F. State of the Art and Perspectives of Hierarchical Zeolites: Practical Overview of Synthesis Methods and Use in Catalysis. *Adv. Mater.* **2020**, *32*, e2004690. [[CrossRef](#)] [[PubMed](#)]

23. Martins, A.; Neves, V.; Moutinho, J.; Nunes, N.; Carvalho, A.P. Friedel-Crafts acylation reaction over hierarchical Y zeolite modified through surfactant mediated technology. *Microporous Mesoporous Mater.* **2021**, *323*, 111167. [[CrossRef](#)]
24. Escola, J.M.; Serrano, D.P.; Sanz, R.; Garcia, R.A.; Peral, A.; Moreno, I.; Linares, M. Synthesis of hierarchical Beta zeolite with uniform mesopores: Effect on its catalytic activity for veratrole acylation. *Catal. Today* **2018**, *304*, 89–96. [[CrossRef](#)]
25. Manrique, C.; Guzmán, A.; Pérez-Pariente, J.; Márquez-Álvarez, C.; Echavarría, A. Vacuum gas-oil hydrocracking performance of Beta zeolite obtained by hydrothermal synthesis using carbon nanotubes as mesoporous template. *Fuel* **2016**, *182*, 236–247. [[CrossRef](#)]
26. Zhang, J.; Wang, L.; Wang, G.; Chen, F.; Zhu, J.; Wang, C.; Bian, C.; Pan, S.; Xiao, F.-S. Hierarchical Sn-Beta Zeolite Catalyst for the Conversion of Sugars to Alkyl Lactates. *ACS Sustain. Chem. Eng.* **2017**, *5*, 3123–3131. [[CrossRef](#)]
27. Zhao, D.; Wang, Y.; Chu, W.; Wang, X.; Zhu, X.; Li, X.; Xie, S.; Wang, H.; Liu, S.; Xu, L. Direct synthesis of hollow single-crystalline zeolite beta using a small organic lactam as a recyclable hollow-directing agent. *J. Mater. Chem. A* **2019**, *7*, 10795–10804. [[CrossRef](#)]
28. Zheng, K.; Liu, B.; Huang, J.; Zhang, K.; Li, F.; Xi, H. Cationic surfactant-directed synthesis of hollow Beta zeolite with hierarchical structure. *Inorg. Chem. Commun.* **2019**, *107*, 107468. [[CrossRef](#)]
29. Möller, K.; Yilmaz, B.; Müller, U.; Bein, T. Hierarchical Zeolite Beta via Nanoparticle Assembly with a Cationic Polymer. *Chem. Mater.* **2011**, *23*, 4301–4310. [[CrossRef](#)]
30. Zhang, K.; Liu, Z.; Wang, M.; Yan, X.; Li, C.; Xi, H. Synthesis and catalytic performance of hierarchically structured beta zeolites by a dual-functional templating approach. *New J. Chem.* **2017**, *41*, 3950–3956. [[CrossRef](#)]
31. Zhu, J.; Liu, Z.; Sukenaga, S.; Ando, M.; Shibata, H.; Okubo, T.; Wakihara, T. Ultrafast synthesis of \*BEA zeolite without the aid of aging pretreatment. *Microporous Mesoporous Mater.* **2018**, *268*, 1–8. [[CrossRef](#)]
32. Al-Eid, M.; Ding, L.; Saleem, Q.; Badairy, H.; Sitepu, H.; Al-Malki, A. A facile method to synthesize hierarchical nano-sized zeolite beta. *Microporous Mesoporous Mater.* **2019**, *279*, 99–106. [[CrossRef](#)]
33. Bok, T.O.; Andriako, E.P.; Knyazeva, E.E.; Ivanova, I.I. Engineering of zeolite BEA crystal size and morphology via seed-directed steam assisted conversion. *RSC Adv.* **2020**, *10*, 38505–38514. [[CrossRef](#)]
34. Sun, M.-H.; Chen, L.-H.; Yu, S.; Li, Y.; Zhou, X.-G.; Hu, Z.-Y.; Sun, Y.-H.; Xu, Y.; Su, B.-L. Micron-Sized Zeolite Beta Single Crystals Featuring Intracrystal Interconnected Ordered Macro-Meso-Microporosity Displaying Superior Catalytic Performance. *Angew. Chem. Int. Ed.* **2020**, *59*, 19582–19591. [[CrossRef](#)] [[PubMed](#)]
35. Miao, S.; She, P.; Chang, X.; Zhao, C.; Sun, Y.; Lei, Z.; Sun, S.; Zhang, W.; Jia, M. Synthesis of beta nanozeolite aggregates with hierarchical pores via steam-assisted conversion of dry gel and their catalytic properties for Friedel-Crafts acylation. *Microporous Mesoporous Mater.* **2022**, *334*, 111777. [[CrossRef](#)]
36. Soltanali, S.; Darian, J.T. Synthesis of mesoporous beta catalysts in the presence of carbon nanostructures as hard templates in MTO process. *Microporous Mesoporous Mater.* **2019**, *286*, 169–175. [[CrossRef](#)]
37. Egeblad, K.; Kustova, M.; Klitgaard, S.K.; Zhu, K.; Christensen, C.H. Mesoporous zeolite and zeotype single crystals synthesized in fluoride media. *Microporous Mesoporous Mater.* **2007**, *101*, 214–223. [[CrossRef](#)]
38. Truong, T.T.T.; Vu, T.N.; Dinh, T.D.; Pham, T.T.; Nguyen, T.A.H.; Nguyen, M.H.; Nguyen, T.D.; Yusa, S.-I.; Pham, T.D. Adsorptive removal of cefixime using a novel adsorbent based on synthesized polycation coated nanosilica rice husk. *Prog. Org. Coat.* **2021**, *158*, 106361. [[CrossRef](#)]
39. Nguyen, Q.K.; Hoang, T.H.; Bui, X.T.; Nguyen, T.A.H.; Pham, T.D.; Pham, T.N.M. Synthesis and application of polycation-stabilized gold nanoparticles as a highly sensitive sensor for molecular cysteine determination. *Microchem. J.* **2021**, *168*, 106481. [[CrossRef](#)]
40. Xiao, F.S.; Wang, L.; Yin, C.; Lin, K.; Di, Y.; Li, J.; Xu, R.; Su, D.S.; Schlogl, R.; Yokoi, T.; et al. Catalytic properties of hierarchical mesoporous zeolites templated with a mixture of small organic ammonium salts and mesoscale cationic polymers. *Angew. Chem. Int. Ed. Engl.* **2006**, *45*, 3090–3093. [[CrossRef](#)]
41. Zhu, J.; Zhu, Y.; Zhu, L.; Rigutto, M.; van der Made, A.; Yang, C.; Pan, S.; Wang, L.; Zhu, L.; Jin, Y.; et al. Highly mesoporous single-crystalline zeolite beta synthesized using a nonsurfactant cationic polymer as a dual-function template. *J. Am. Chem. Soc.* **2014**, *136*, 2503–2510. [[CrossRef](#)]
42. Du, S.; Sun, Q.; Wang, N.; Chen, X.; Jia, M.; Yu, J. Synthesis of hierarchical TS-1 zeolites with abundant and uniform intracrystalline mesopores and their highly efficient catalytic performance for oxidation desulfurization. *J. Mater. Chem. A* **2017**, *5*, 7992–7998. [[CrossRef](#)]
43. Du, S.; Chen, X.; Sun, Q.; Wang, N.; Jia, M.; Valtchev, V.; Yu, J. A non-chemically selective top-down approach towards the preparation of hierarchical TS-1 zeolites with improved oxidative desulfurization catalytic performance. *Chem. Commun.* **2016**, *52*, 3580–3583. [[CrossRef](#)]
44. Song, X.; Yang, X.; Zhang, T.; Zhang, H.; Zhang, Q.; Hu, D.; Chang, X.; Li, Y.; Chen, Z.; Jia, M.; et al. Controlling the Morphology and Titanium Coordination States of TS-1 Zeolites by Crystal Growth Modifier. *Inorg. Chem.* **2020**, *59*, 13201–13210. [[CrossRef](#)]
45. Miao, S.; Liu, Y.; Zhang, H.; Chang, X.; Sun, H.; Zhao, C.; Zhang, W.; Jia, M. Effect of Triton X-100 additive on the synthesis of Beta zeolites and their catalytic application in acylation of anisole with acetic anhydride. *Mater. Chem. Phys.* **2021**, *278*, 125618. [[CrossRef](#)]
46. Treacy, M.M.J.; Newsam, J.M. Two new three-dimensional twelve-ring zeolite frameworks of which zeolite beta is a disordered intergrowth. *Nature* **1988**, *322*, 249–251. [[CrossRef](#)]

47. Wang, L.; Zhang, Z.; Yin, C.; Shan, Z.; Xiao, F.-S. Hierarchical mesoporous zeolites with controllable mesoporosity templated from cationic polymers. *Microporous Mesoporous Mater.* **2010**, *131*, 58–67. [[CrossRef](#)]
48. Bisio, C.; Martra, G.; Coluccia, S.; Massiani, P. FT-IR Evidence of Two Distinct Protonic Sites in BEA Zeolite Consequences on Cationic Exchange and on Acido-Basic Properties in the Presence of Cesium. *J. Phys. Chem. C* **2008**, *112*, 10520–10530. [[CrossRef](#)]
49. Maier, S.M.; Jentys, A.; Lercher, J.A. Steaming of Zeolite BEA and Its Effect on Acidity: A Comparative NMR and IR Spectroscopic Study. *J. Phys. Chem. C* **2011**, *115*, 8005–8013. [[CrossRef](#)]
50. Wang, W.; Zhang, W.; Chen, Y.; Wen, X.; Li, H.; Yuan, D.; Guo, Q.; Ren, S.; Pang, X.; Shen, B. Mild-acid-assisted thermal or hydrothermal dealumination of zeolite beta, its regulation to Al distribution and catalytic cracking performance to hydrocarbons. *J. Catal.* **2018**, *362*, 94–105. [[CrossRef](#)]
51. Wei, H.; Liu, K.; Xie, S.; Xin, W.; Li, X.; Liu, S.; Xu, L. Determination of different acid sites in Beta zeolite for anisole acylation with acetic anhydride. *J. Catal.* **2013**, *307*, 103–110. [[CrossRef](#)]
52. Rohan, D.; Canaff, C.; Fromentin, E.; Guisnet, M. Acetylation of anisole by acetic anhydride over a HBEA zeolite—Origin of deactivation of the catalyst. *J. Catal.* **1998**, *177*, 296–305. [[CrossRef](#)]
53. Zhao, D.; Wang, J.; Zhang, J. Effects of Modified Beta Zeolites with Acid on Anisole Acetylation in a Fixed Bed Reactor. *Catal. Lett.* **2008**, *126*, 188–192. [[CrossRef](#)]
54. Alalq, I.; Nguyen-Phu, H.; Crossley, S. Shifts in catalyst deactivation mechanisms as a function of surface coverage during Friedel-Crafts acylation in zeolites. *J. Catal.* **2023**, *426*, 222–233. [[CrossRef](#)]
55. Liu, Z.; Dong, X.; Zhu, Y.; Emwas, A.-H.; Zhang, D.; Tian, Q.; Han, Y. Investigating the Influence of Mesoporosity in Zeolite Beta on Its Catalytic Performance for the Conversion of Methanol to Hydrocarbons. *ACS Catal.* **2015**, *5*, 5837–5845. [[CrossRef](#)]
56. Wang, Y.; Otomo, R.; Tatsumi, T.; Yokoi, T. Dealumination of organic structure-directing agent (OSDA) free beta zeolite for enhancing its catalytic performance in n-hexane cracking. *Microporous Mesoporous Mater.* **2016**, *220*, 275–281. [[CrossRef](#)]
57. Kim, J.; Choi, M.; Ryoo, R. Effect of mesoporosity against the deactivation of MFI zeolite catalyst during the methanol-to-hydrocarbon conversion process. *J. Catal.* **2010**, *269*, 219–228. [[CrossRef](#)]
58. Derouane, E.G.; Dillon, C.J.; Bethell, D.; Hamid, S.B.D.-A. Zeolite Catalysts as Solid Solvents in Fine Chemicals Synthesis\_1. Catalyst Deactivation in the Friedel–Crafts Acetylation of Anisole. *J. Catal.* **1999**, *187*, 209–218. [[CrossRef](#)]

**Disclaimer/Publisher’s Note:** The statements, opinions and data contained in all publications are solely those of the individual author(s) and contributor(s) and not of MDPI and/or the editor(s). MDPI and/or the editor(s) disclaim responsibility for any injury to people or property resulting from any ideas, methods, instructions or products referred to in the content.